Continuous hydrothermal flow synthesis of blue-luminescent, excitation-independent nitrogen-doped carbon quantum dots as nanosensors†

Ioan-Alexandru Baragau, [a] Nicholas P. Power, [b] David J. Morgan, [c]
Tobias Heil, [d] Richard Alvarez Lobo, [e] Christopher Simon Roberts, [f]
Maria-Madgalena Titirici, [e] Steven Dunn [a] and Suela Kellici [*a]

Blue-luminescent N-doped carbon quantum dots (NCQDs) exhibiting rarely observed excitation independent optical properties are synthesised from citric acid in the presence of ammonia via a Continuous Hydrothermal Flow Synthesis (CHFS) approach. CHFS is an eco-friendly, rapid synthetic approach (within fractions of a second) facilitating ease of scale-up industrialization as well as offering materials with superior properties. The synthesised NCQDs readily disperse in aqueous solution, have an average particle size of 3.3 0.7 nm, with highest emission intensity at 441 nm (and a narrow full width at half maximum, FWHM 78 nm) under a 360 nm excitation wavelength. N-doped carbon quantum dots, without any further modification, exhibited a high selectivity and sensitivity as a nano-sensor for the highly toxic and carcinogenic chromium(VI) ions. The nano-chemo-sensor delivers significant advantages including simplicity of manufacturing via a continuous, cleaner technology (using targeted biomass precursor), high selectivity, sensitivity and fast response leading to potential applications in environmental industry as well photovoltaics, bio-tagging, bio-sensing and beyond.

Introduction

Fluorescent carbon quantum dots (CQD) typically with particle size < 10 nm in diameter, quasi-spherical, and discrete morphological structure, have attracted increasing scienti c and industrial interest over the last decade. In possessing either a core of graphite or an amorphous carbon framework (hybri-dised sp^2/sp^3), with a surface that can be richly coated with functional groups (e.g. oxygen moieties), polymers or other derivative species (all dependant on the synthetic route and the carbon source), CQDs offer a range of potential properties such as high photostability, good biocompatibility, and excellent optical properties, with low potential for environmental hazards.[1,2] As such, CQDs are excellent candidates in a variety of applications including bio-imaging & bio-tagging,[3,4] drug delivery,[5,6] uorescent ink,[7] ion sensors,[8,9] optoelectronics,[10] photocatalysis,[11] light-emitting devices,[12] and solar cells.[13]

Currently, there is signi cant interest in the bottom-up methodologies[14–17] which utilise biomass resources as targeted precursors (e.g. citric acid, glucose) for conversion into nano-sized carbon dots[1,18] via intra- or inter-dehydration and/or decomposition processes. Contrary to the top-down route (derived from cutting larger dimensional pre-made parent precursors such as carbon nanotubes or graphite for example),[19] the alternative bottom-up approaches can offer "one pot" surface functionalisation via selective heteroatom doping (e.g. nitrogen)[20] to give highly uorescent materials without further need of a post-synthesis treatment (typical for top-down approaches). However, the current bottom-up approaches have their own challenges including lengthy manufacturing time, non-uniformity in CQD particle size distribution, inconsistent reproducibility and high energy costs. Consequently, applying the aforementioned synthetic approaches to an industrial scale within the current parameters would be limiting. In this regard, overcoming these challenges in providing a controllable, cleaner and rapid synthetic process with potential for industrial scale-up, as well delivering high-performance CQD is important.

It is in this context, Continuous Hydrothermal Flow Synthesis (CHFS), is highlighted[21–27] as one of the most prom-ising methods employed for the bottom-up approach offering

[a] School of Engineering, London South Bank University, 103 Borough Road, London, SE1 0AA, UK. E-mail: kellicis@lsbu.ac.uk; Web: www.nano2d.co.uk

[b] School of Life Health & Chemical Sciences, Open University, Walton Hall, Milton Keynes, MK7 6AA, UK

[c] Cardiff Catalysis Institute, School of Chemistry, Cardiff University, Park Place, Cardiff, CF10 3AT, UK

[d] Department of Colloid Chemistry, Max Planck Institute of Colloids and Interfaces, Am Muhlenberg¨ 1, 14476 Potsdam, Germany

[e] Department of Chemical Engineering, Imperial College, South Kensington, London, SW7 2AZ, UK

[f] Department of Chemistry, Imperial College, South Kensington, London, SW7 2AZ, UK

† Electronic supplementary information (ESI) available. See DOI: 10.1039/c9ta11781d

signi cant synthetic advantages over traditional methods, delivering in a cleaner and rapid mode, high-quality nanosized materials. The CHFS process involves mixing a feed of super-critical water (374 C, 22.1 MPa) with target precursor feed/s in the reaction zone, with reaction times approaching fractions of a second to give the desired product. The resulting treated reaction mixture passes through a cooler and the product is collected as an aqueous nanomaterial suspension. Compared with traditional hydrothermal methods, the CHFS process consumes less energy and time,[21,27] delivering quality and reproducibility of a homogenous product, whilst offering in real time full control and tunability of the reaction parame-ters.[21,26,28–30] The unique synthetic properties of CHFS method have previously been applied to the continuous hydrothermal ow synthesis of graphene quantum dots (rst in this eld)[29] adding to the portfolio of CHFS materials delivered by our group. We have also reported the substantially lower environ-mental impact of CHFS when compared to equivalent batch hydrothermal processes used for the synthesis of graphene quantum dots.[27] The current work adds further to the devel-opment of continuous ow technology of carbon related quantum dots nanomaterial.

One of the unique and interesting features of heteroatom doped CQDs is their selectivity, sensitivity and response to ions and molecular compounds in solution that result in changes in optical behaviour (uorescence enhancement or quenching).[31] Their response is reported to be highly dependent on the structure of the carbon dots, in particular their surface struc-ture.[31] Reported literature examples of luminescent doped CQDs have been successfully tested as uorescent nano-sensors for pH,[32] ions (Fe(II/III),[9] Cr(VI),[33] Cu(III)[9,31,34]) and molecular compounds.[35] Herein, we will explore the sensing properties of the NCQD for chromium(VI) detection. Cr(IV) contamination of soil and water is anthropogenic in origin and raises signi cant concern in both developed and developing countries as a hazardous pollutant to the environment and human life, due to its high toxicity, carcinogenicity and mutagenic behaviour compared to other valence states, such as Cr(0) and Cr(III).[36–38] Thus, the detection/concentration determination of Cr(VI) in drinking water (rigorously regulated to a very low micromolar level) for example, is vital.[36,39] The current techniques of analysis (atomic absorption spectrometry, chromatography) have common challenges including time consuming complex pre-treatment procedures and/or use of costly equipment. There-fore, a low cost, highly sensitive and selective sensor for the detection and determination of Cr(VI) is needed, particularly in regions that are underdeveloped or lacking scal capability or access to such facilities.

Herein, we report a facile, green, one-step continuous hydro-thermal ow synthesis route using inexpensive and simple precursors; citric acid as a carbon source and ammonia, for production of blue emission N-doped carbon quantum dots that can be utilised as chemisensors for Cr(VI) detection. The synthesis of N-doped CQDs (NCQD) via the CHFS system delivers the following advantages: (a) from a series of synthetic stages to a single step approach (synthesis and simultaneous doping), (b) a signi cant reduction in reaction times from hours to seconds,

thereby reducing energy consumption, (c) promoting the use of renewable precursors (citric acid) and solvent (water), (d) facili-tating tunability and control over reaction parameters (e.g. temperature, pressure and ow rate) and hence particle proper-ties, (e) as well as easy industrial scalability. Applying CHFS methods to produce carbon-based materials from biomass derivatives offers a new direction in achieving large-scale production of homogenous quality NCQDs with potentially signi cant reduced costs and lower environmental impact.

Experimental section

Chemicals

All the materials were purchased from commercial suppliers and used without further puri cation. Deionised water, 15 MΩ obtained from an ELGA Purelab system was used in all experi-ments. Anhydrous citric acid, ammonia (32%) and Cr(VI) (potassium chromate and potassium dichromate) were purchased from Fisher Chemicals (UK) and used as received. The solutions of metal ions were prepared from their nitrate,

acetate or chloride salts. The chlorides of Na^+, K^+, acetate of Fe^{2+}, Zn^{2+}, Cu^{2+}, nitrates of Ce^{3+}, Co^{2+}, Ni^{2+}, Ag^+ and sodium: F , Cl , Br , I , NO_3 , SO_4^{2} and HCO_3 were all purchased from Sigma Aldrich (UK).

Equipment

Freeze-drying was performed using a Heto PowderDry PL 3000. X-ray photoelectron spectroscopy (XPS). XPS measurements were performed using a Kratos Axis Ultra DLD photoelectron spectrometer utilizing monochromatic Alka source operating at 144 W. Samples were mounted using conductive carbon tape. Survey and narrow scans were performed at constant pass energies of 160 and 40 eV, respectively. The base pressure of the system was ca. 1×10^{9} Torr rising to ca. 4×10^{9} Torr under the analysis of these samples.

High-resolution transmission electron microscopy (HRTEM). Double-corrected JEOL ARM200F, equipped with a cold eld emission gun. For the investigation, the acceleration voltage has been set to 80 kV and the emission was set to 10 mA. The samples were prepared by depositing the aqueous solution of NCQDs onto a holey carbon coated Cu-grid (400 mm). The particle size of carbon quantum dots was measured from TEM images using ImageJ so ware.

Fourier-transform infrared spectroscopy (FT-IR). FT-IR spectra were recorded using a Nicolet Avatar 370DTGS spec-trometer tted with a Smart Orbit accessory (diamond 4000– 200 cm^{1}).

Raman spectroscopy. The spectrum of the as-synthesised and dried carbon quantum dots was measured with a Horiba LabRAM HR Evolution spectrometer with radiation at 514 nm.

Atomic Force Microscopy (AFM) images were obtained via dynamic mode on a hpAFM with AFM Controller (Nano-Magnetics Instruments, UK) using Nanosensor tapping mode probes. The micrographs were then processed with NMI Image Analyser (v1.4, NanoMagnetics Instruments), with plane correction and scar removal using the in-built functions.

Steady-state optical characterisation. A er the sample was puri ed, it was optically characterized using absorption (UV-Vis spectrophotometry) and emission/excitation (photo-luminescence spectrophotometry) techniques. The sample concentration (1.1 mg mL^{1}) was determined by freeze-drying 10 mL of the puri ed carbon dot sample.

UV-Vis spectrophotometry. Adsorption measurements were conducted using a Shimadzu UV-1800, in the range of 200– 700 nm in a 10 mm quartz cuvette.

Photoluminescence spectroscopy (PL). The uorescence spectra were recorded with Shimadzu RF-6000 Spectro uorophotometer.

Quantum yield (QY) determination. QY value of carbon quantum dots was calculated by measuring the integrated PL intensity in aqueous dispersion of NCQDs in comparation with the integrated PL of quinine sulphate in 0.1 M H_2SO_4 (stan-dard), and was plotted as integrated PL vs. Absorbance (Fig. S1†) from which the extracted slopes (the gradient D) were obtained.

where q_{QDs} is the quantum yield of NCQDs; q_S is the quantum yield of standard (quinine sulphate 54%); D_{QDs} is the slope of integrated PL of NCQDs; D_S is the slope of integrated PL intensity of the standard; h_{QDs} is the refractive index of water (1.33); h_S is the refractive index of 0.1 M H_2SO_4 (1.33).

Fluorescence experiments

Fluorescence sensitivity and selectivity experiments of N-doped carbon quantum dots with Cr(VI) were performed as follows: Cr(VI) stock solution (1000 ppm) was prepared by dissolving potassium chromate (K_2CrO_4, 100 mg) in NCQD aqueous solu-tion (100 mL) in a standard volumetric ask. Further, fresh NCQD solution (1.1 mg mL^{1}) was placed into a 10 mL standard volumetric ask, followed by addition of a required volume of 1000 ppm Cr(VI) stock solution to achieve concentrations of 500 ppm, 250 ppm, 100 ppm, 75 ppm, 50 ppm, 20 ppm, 10 ppm, and 5 ppm. Additional dilutions of Cr(VI) in the ppb concen-tration range were prepared from Cr(VI) 100 ppm solution giving the following concentrations: 5 ppb, 10 ppb, 20 ppb, 50 ppb, 100 ppb, and 500 ppb (Fig. S2†). A er 3 minutes incubation and stirring at room temperature, the uorescence spectra were measured for the quantitative analysis of Cr(VI). Each experi-ment was repeated in triplicate. The uorescence emission spectra for ion-sensing experiments were recorded for excita-tion at 360 nm with the band-slits of both excitation and emission set as 5 nm. The sensitivity was xed on high with a response time set at 0.5 s. The emission spectra were recorded from 300 to 650 nm, and the uorescence intensity of NCQDs at 441 nm was used for quantitative analysis of Cr(VI). For comparison purposes, a range of anions and various metal cations were tested for selectivity and sensitivity using 50 ppm as a standard concentration. Furthermore, stability analysis of the NCQDs in presence of Cr(VI) (50 ppm) were conducted by recording the uorescence intensity of the mixture when initially exposed continuously for 5400 seconds (90 minutes) at

Synthetic methodology

Synthesis of NCQDs. The experimental procedure for NCQDs produced via the CHFS approach is depicted in Scheme 1. Optimally for this study, CHFS consisted of three feeds: super-critical water feed (F1: ow rate of 20 mL min^{1}) and two feeds of the precursors: citric acid (F2: with concentration of 70 mg mL^{1} delivered at 10 mL min^{1} in the mixing zone) and ammonia (F3: with concentration of 1 M pumped at 10 mL min^{1}). The supercritical water feed was heated at 450 C (lower temperatures of 250 C and 350 C have also been explored) and the system pressure was kept constant at 24.8 MPa using a back-pressure regulator (labelled as BPR). Feeds F2 and F3 were combined in a "T" junction prior to being delivered into the reaction zone (labelled as "Reactor") where it was mixed with the supercritical water feed (F1). The reaction

$$q_{QDs} = q_s \, D_s \, \frac{h_s}{\nu_{QDs}} \cdot \frac{}{n_{QDs}} \, 2 \tag{1}$$

(1) mixture was then passed via the "Cooler" to the BPR (back-pressure regulator) and collected for further processing (see Scheme 1). The entire reaction mixture was ltered using 0.2 mm alumina membrane, and the ltrate was initially separated using 30 kD membrane in a tangential ltration unit, followed by 1 kD membrane. The resulting solution was concentrated to 1/5 of the initial volume and subjected to further analysis.

Results and discussion

Carbon dots are known for their properties, speci cally their intense uorescence in the visible range.[7,13,20] However, the materials o en exhibit optical and structural heterogeneity as well as limited relevant synthetic approaches that do not readily facilitate large-scale production. We have explored and devel-oped a rapid synthesis approach that delivers in a continuous mode, carbon quantum dots (control) and blue luminescent N-doped carbon quantum dots by simply using citric acid (carbon source), in the absence and presence of ammonia (N-precursor) respectively, both in water under supercritical conditions (24.8 MPa and study reaction temperatures of 250 C, 350 C and 450 C). The optimal temperature was 450 C for the NCQDs (see Fig. S4†) synthesised using continuous hydrothermal ow synthesis (a single step approach as shown in Scheme 1) showing high homogeneity (narrow particle size distribution) and excellent optical properties (excitation independent uorescence).

The optimal as-produced NCQDs were characterized using a variety of techniques including UV-Vis absorption and emis-sion (PL) spectrophotometry to examine the optical properties, FT-IR and Raman spectroscopy to determine electronic prop-erties and functionalities, X-ray photoelectron spectroscopy (XPS) to determine the composition and surface chemistry, high-resolution transmission electron microscopy (HRTEM) analysis and atomic force microscopy (AFM) for particle size analysis and structural morphology.
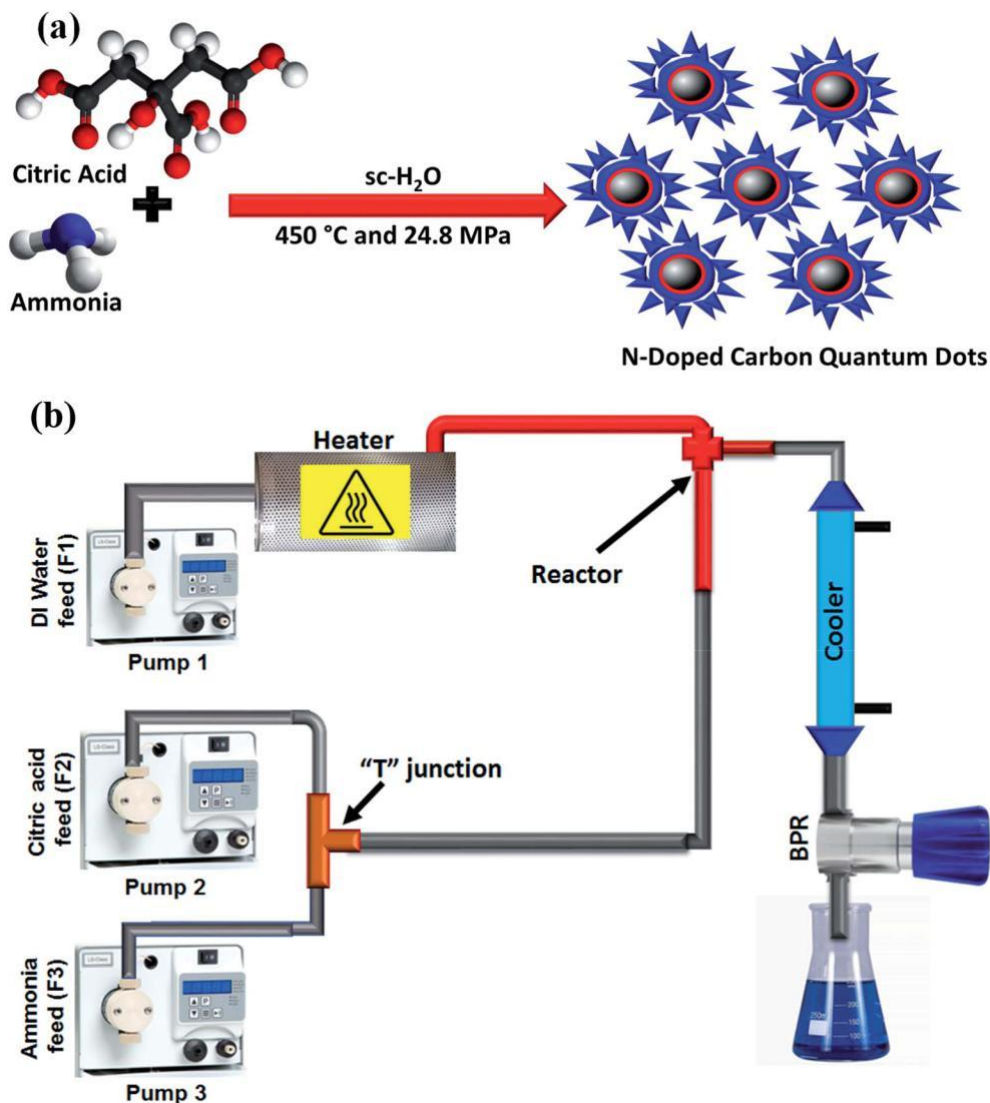
HRTEM images (Fig. 1) of the as-prepared NCQDs exhibit a quasi-spherical morphology with an average particle size of

Scheme 1 Synthesis of N-doped carbon quantum dots (NCQDs) using Continuous Hydrothermal Flow Synthesis (CHFS) process: (a) illustration of the CHFS synthesis process using citric acid as carbon source and ammonia as N-dopant, (b) simplified CHFS design.

3.3 0.7 nm from a sample population of 190 particles ranging between 1.9 nm to 4.7 nm in diameter (inset Fig. 1b). Each exhibited the same structural arrangement, indicating a consistency in homogeneity for the CHFS synthesized sample. The graphitic core arrangement of the carbon atoms (Fig. 1c) can be clearly identi ed with in-plane lattice spacing of 0.22 nm and is consistent with the reported literature data.[40]

The atomic force microscopy (AFM) image (Fig. 1d) reveals the tomography of the as-synthesised NCQDs, distributed in the range from 1.0 to 5.2 nm, with an average value of 2.4 1.0 nm, and is consistent (within experimental error) with data from HRTEM.

X-ray photoelectron spectroscopy (XPS) measurements were performed for the surface characterization of NCQDs (Fig. 2a) and reveal peaks typical for the presence of carbon (ca. 285 eV), nitrogen (ca. 399 eV) and oxygen (ca. 531 eV). The tted C1s spectra (Fig. 2b) peaks at 284.9 eV, 285.9 eV, and 288.4 eV can be assigned to the carbon atoms in the form of C]C bond (sp^2), C–N (sp^3), C]O (sp^2) and O–C]O (sp^2), respectively, whilst the tted N(1s) spectrum (Fig. 2c) exhibits three peaks at 399.7 eV, 400.8 eV, and 401.6 eV, indicating that the nitrogen exists in pyrollic/amino N–H, protonated pyridinic N, and graphitic-N (sp^3) forms respectively, signifying that the nitrogen atoms were efficiently doped into the structure.[41] Elemental analysis (inset Fig. 2a) shows that CHFS synthesised NCQDs contain 35.9 wt% oxygen, 10.8 wt% nitrogen and 53.3 wt% of carbon, concluding that NCQDs are nitrogen-doped and carbon-rich.

The Raman spectrum for the NCQDs (Fig. 3a) displayed two broad peaks at 1392 and 1591 cm^{-1} which correspond to the D and G bands, respectively. The G band is attributed to an E_{2g} mode of vibration of sp^2 bonded carbon atoms associated with the graphitic core and is in good agreement with the HRTEM lattice spacing image described previously for the NCQDs (Fig. 1c). The smaller D band peak is due to the presence of
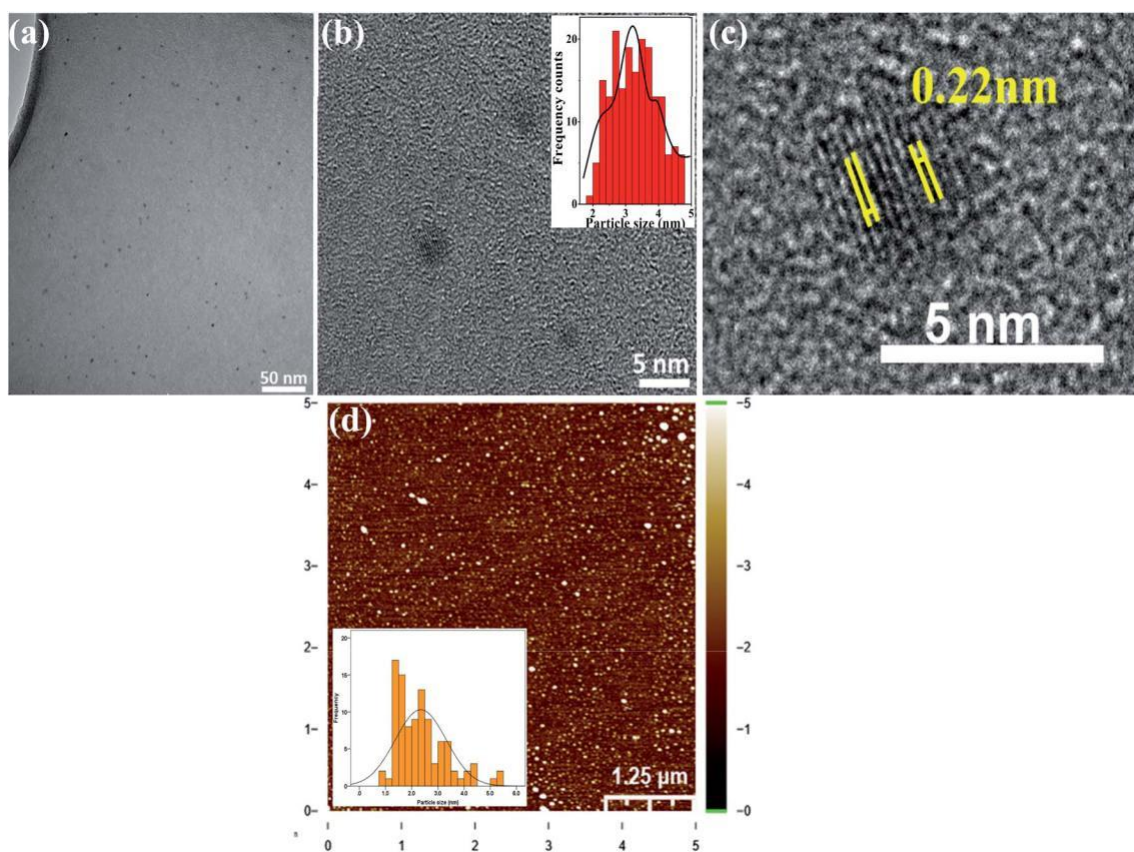
Fig. 1 HRTEM images of N-doped carbon quantum dots at different magnification and scale: (a) 50 nm, (b) 5 nm with (inset) showing particle size distribution histogram with an average particle size of 3.3 0.7 nm, (c) graphitic core lattice fringes, (d) AFM image with inset showing particle size distribution histogram.

a medium level of oxygen content (35.9 wt%) and the presence of sp^3 carbon atoms, the results are complimentary with the XPS data (see Fig. 2). The relative intensity ratio of the observed bands (I_D/I_G) gave a value of 0.76 for the NCQDs, typical of graphene oxide.[30]

The FT-IR spectroscopy (Fig. 3b) further supports the XPS analysis. A broad absorption band (3450–2400 cm^1) can be ascribed to overlapping stretches that encompass those for O–H (R–OH, –COOH), amine and protonated amine (N–H$^+$, N–H^{2+}, N–H^{3+}) stretches, and C–H stretching vibrations (3028 cm^1 and 2835 cm^1). The presence of protonated and deprotonated species is plausible with carboxylates and amine groups in close proximity on the NCQDs. Other stretches observed include pyridinic C]N at 1652 cm^1, a stretch which could also be attributed to an amino-vibration (–NH or –NH$_2$). The amino vibrations could also be assigned for stretches at 864 cm^1 and 792 cm^1 as well as carbonyl (COO–) stretches at 1541 cm^1 and 1394 cm^1, asymmetric vibrations for C–NH–C at 1136 cm^1, and C–O and C–O–C vibrations may be assigned to stretches at 1202 cm^1 and 1035 cm^1, respectively.[41]

The NCQDs were analysed with UV-Vis and the steady-state PL spectrophotometry. The characteristic speci c absorption (black curve) and emission bands (red curve) recorded from aqueous solutions of NCQDs are shown in Fig. 4. Fig. 4(a) shows the strongest absorbance and emission band for NCQDs

produced via CHFS. The UV-Vis spectrum displays two absorp-tion bands that are characteristic of NCQDs, the rst at 250 nm and the second peaking at 332 nm (broad absorption band from 300 nm tailing to 480 nm). The former band can be ascribed to p–p* transitions for aromatic sp^2 domains in the graphitic core and the latter to n–p* transitions for C]O in the NCQDs.[19,42] The absorption band displayed below 250 nm can be attributed to the C]C and the C–C bonds. Photoluminescence (PL) was observed for both the as-prepared NCQDs and the CQDs (control) under UV excitation with wavelengths ranging from 300–420 nm. The control material, CQDs synthesised from citric acid only, showed negligible photoluminescence (see Fig. S4†). The NCQDs on the other hand displayed an optimum excitation at 360 nm corre-sponding to a blue uorescence emission at a consistent 441 nm for each excitation (Fig. 4b), and a red shi lower intensity emission for lower energy excitation at 400 nm and 420 nm. The as-prepared NCQD material exhibited a rarely observed UV excitation independent emission behaviour.[43,44] We attribute this zero-tunability (320–380 nm) behaviour to surface state defects of the NCQDs, which is also commonly associated with blue emission, a feature that has been reported for rGO, GQDs and CNDs. The red shi character due to the observed emission for lower energy excitations may be ascribed to the p–p* transitions (of isolated sp^2 clusters) within the
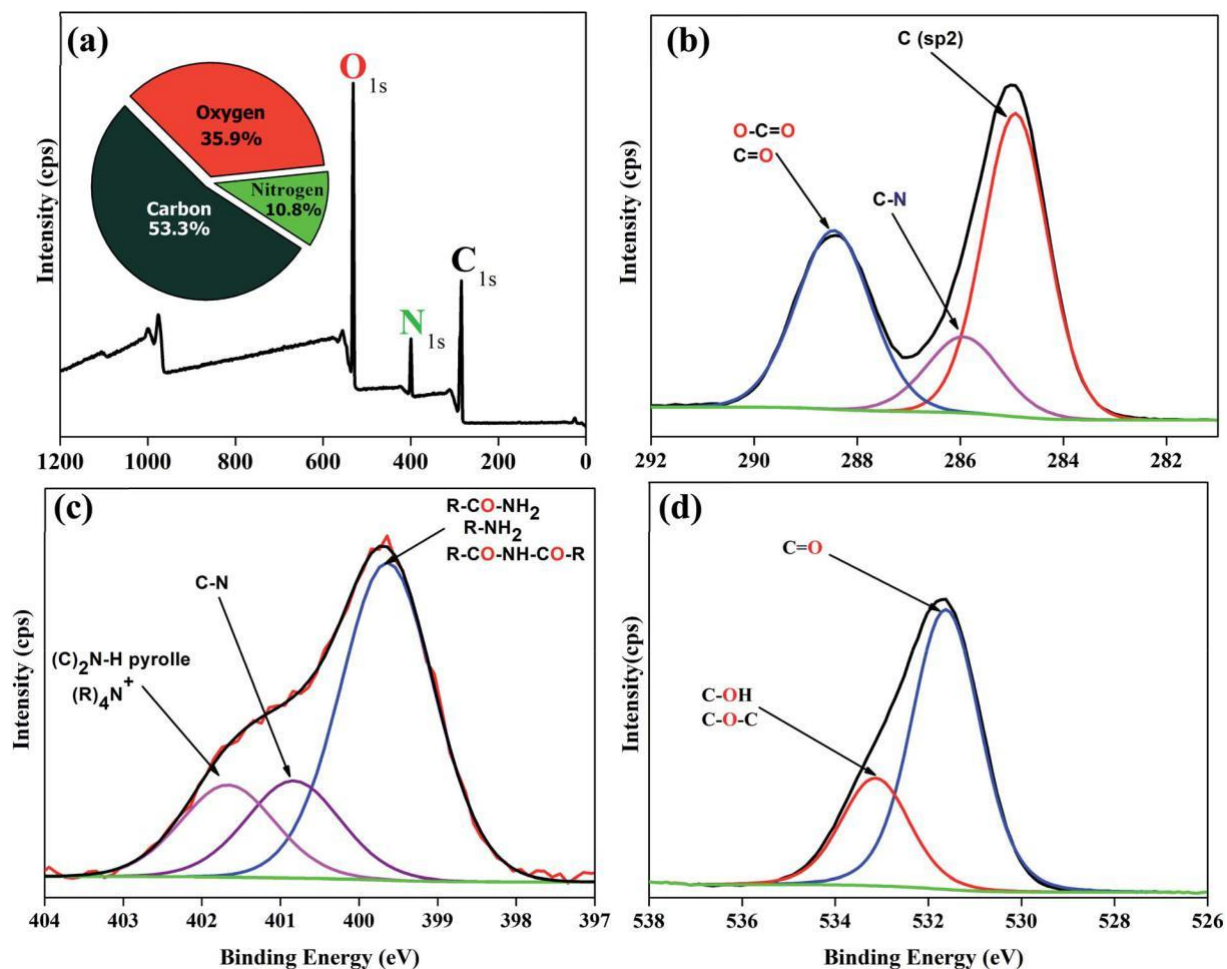
Fig. 2 XPS survey scans of N-doped carbon quantum dots: (a) survey spectrum showing C(1s), N(1s) and O(1s) core levels, (b–d) fitted high resolution spectra of C(1s), N(1s) and O(1s) regions, respectively.

graphitic carbon cores.[45] The proportion of surface defects are correlated with the degree of surface oxidation with the increasing presence of oxygen atoms in the make-up of the surface structure of CQDs which typically leads to further reducing the band gap, i.e. a red shift of PL. However, given the excitation independent blue-luminescent for the as-prepared
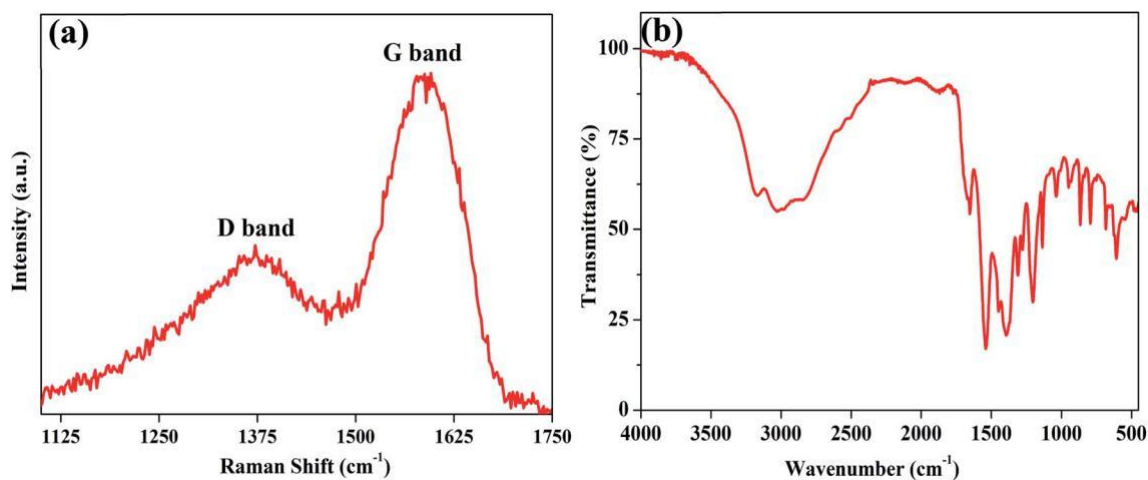

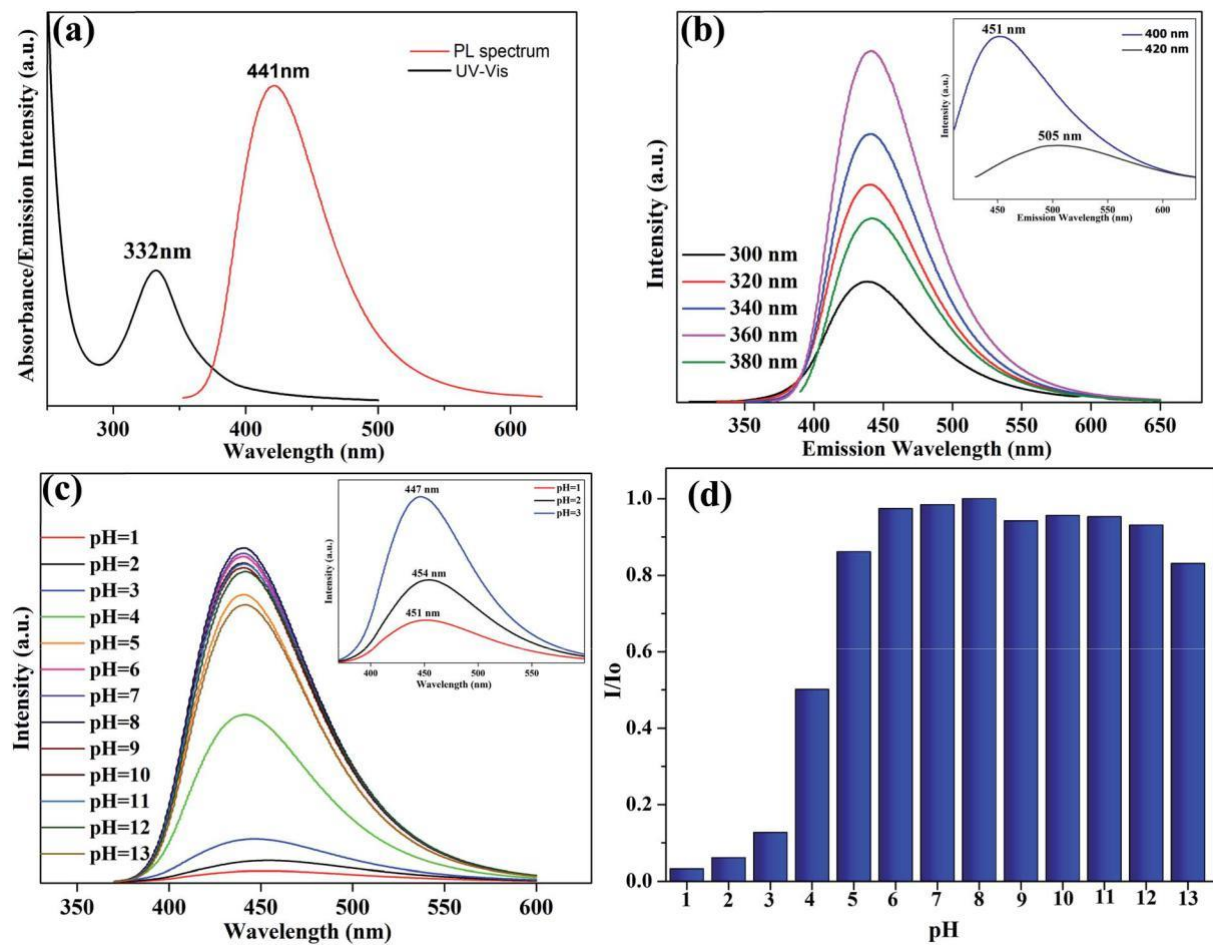Fig. 3 (a) Raman and (b) FTIR spectra of N-doped CQDs.

Fig. 4 (a) UV-Vis absorption spectrum (black curve) and photoluminescence (PL) spectrum (red curve) of carbon quantum dots at 360 nm excitation wavelength. (b) NCQDs excitation at wavelengths 320–380 nm gave emission spectra showing excitation independent optical behaviour, but excitation from 400–420 nm showed excitation dependent behaviour (inset). (c) pH influence over the emission intensity and (d) histogram of pH effect on the emission spectrum.

NCQDs, the process of nitrogen doping (CHFS) as compared to the control, has had a significant impact on the optical prop-erties (Fig. S4†).

Since pH can play pivotal roles in various environmental and biological systems, the impact of pH on the NCQDs perfor-mance as a sensor is of significance. The pH-dependent behaviour of the NCQDs was explored (Fig. 4c and d), where mildly acidic and alkali media have had a small to negligible impact on fluorescence stability showing the NCQDs to be stable over a broad pH range of 5−12. However, the fluorescence intensity of the NCQDs is significantly reduced in acidic media to 50% (against control intensity) at pH 4 and reduced further to just 13% at pH 3 and 3% at pH 1. A small but significant red shift occurs from pH 3 to pH 1. Similar observations have been made by Zhu et al.[8] (for their excitation dependent N-doped CQDs hydrothermally synthesised from citric acid and ethyl-enediamine) and Dong et al.[44] (for the N,S-CQDs) but neither adequately rationalise for the red shift. The diminishing intensity is a consequence of protonation of the nitrogen and carboxylate groups disrupting the surface charge and its asso-ciated emissivity, thus allowing emission from the graphitic

core to come to prominence over that of the surface as reflected by the red shift of the PL. The red-shift feature of the lumi-nescence highlighted earlier is excitation dependent. At pH 13 there is also a reduction in emission intensity versus control. Furthermore, the NCQD material exhibited resistance to photo-bleaching with PL intensity remaining stable over a period of 6 months. The quantum yield value of our sample was measured to be 14.91 0.24% (calibrated against quinine sulphate in 0.1 M H_2SO_4 as standard), comparable to many literature reports for CQDs.[20]

Typically, excitation dependent emission is a common feature of CQDs, but tend to display complex emission spectra that are difficult to decipher in practical applications. Thus, single emission NCQDs are highly desirable. Our CHFS synthesised material uniquely exhibits the following: excitation indepen-dence with a narrow FWHM (78 nm, where 100 nm is typical for CQDs[19]) and a remoteness of the fluorescence emission (441 nm) from the UV excitation range (320–380 nm) – that usefully avoids auto-luminescence. Each of which are desirable features for sensor applications and more so when combined. These char-acteristics will ultimately allow this material to be uniquely

suitable in a range of practical applications, such as chromate anion (Cr(VI)) detection for example; a severe and highly toxic environmental pollutant even at trace (low mg L[1]) levels.

Chromium(VI) ion-sensing

Given the fluorescent properties of the NCQDs and their stability over a broad pH range (pH 5–12), investigations with respect to their interactions with and selectivity for, were undertaken for a range of environmentally relative anions and

cations. These included the metal ions Na^+, K^+, Fe^{2+}, Co^{2+}, Ni^{2+}, Cu^{2+}, Zn^{2+}, Ce^{3+}, Ag^+ and the anions: F^-, Cl^-, Br^-, I^-, NO_3^-, SO_4^{2-}, HCO_3^-, and the Cr(VI) anions CrO_4^{2-} and $Cr_2O_7^{2-}$ at concentrations of 50 ppm each in aqueous solutions.

Sole selectivity for Cr(VI) detection was observed by signi - cant fluorescence quenching of the NCQDs upon the addition of either Cr(VI) species (Fig. 5), whilst the other ions exhibited limited/negligible quenching effect or fluorescence enhance-ment with minimal variation. This selectivity for Cr(VI) (CrO_4^{2-} / $Cr_2O_7^{2-}$) by the NCQDs fluorescent probe was further investi-gated in regard to their sensitivity based on the PL spectra of NCQDs with a range of prepared concentrations of CrO_4^{2-}, each performed in triplicate. As shown in Fig. 6 the fluorescence of NCQDs at around 441 nm is quenched after the addition of

Cr(VI) with the emission intensity shown to be dependent on the concentration of Cr(VI) species. The fluorescence peaks of [CQDs-Cr(VI)] system was stable at 441 nm; no peak shifting was observed.

The fluorescence intensity of NCQDs decreased linearly with concentration of Cr(VI) (Fig. 6). Stern−Volmer relation plot (inset Fig. 6b) showed a good correlation (R^2 ¼ 0.998) giving a quenching constant K_{SV} value of 0.01113 (obtained from the slope of the line y ¼ 0.01113x + 0.03897). The limit of detection (LOD) is calculated as follows: LOD ¼ 3s/K_{SV}, where s is the standard error of the intercept. The LOD obtained value was 0.365 ppm and limit of quanti cation, LOQ ¼ 10s/K_{SV} was
1.218 ppm. Emission intensities at 441 nm for the pure NCQDs and [NCQDs–Cr^{6+}] solutions (Fig. S3†) have shown negligible variation when the samples were continuously excited at 360 nm for 90 minutes. Further interval measurements of [NCQDs–Cr^{6+}] solution revealed just an 8.3% diminishment in emission intensity over a 48 hour period (see Fig. S3†). This stability of the respective systems re ects the materials suit-ability as a sensor for Cr(VI) detection.

Given that there was no observed red-shi for the Cr(VI) studies with the NCQDs, contrary to that to the ndings of the NCQDs pH study, and no observed absorption peak shi s for
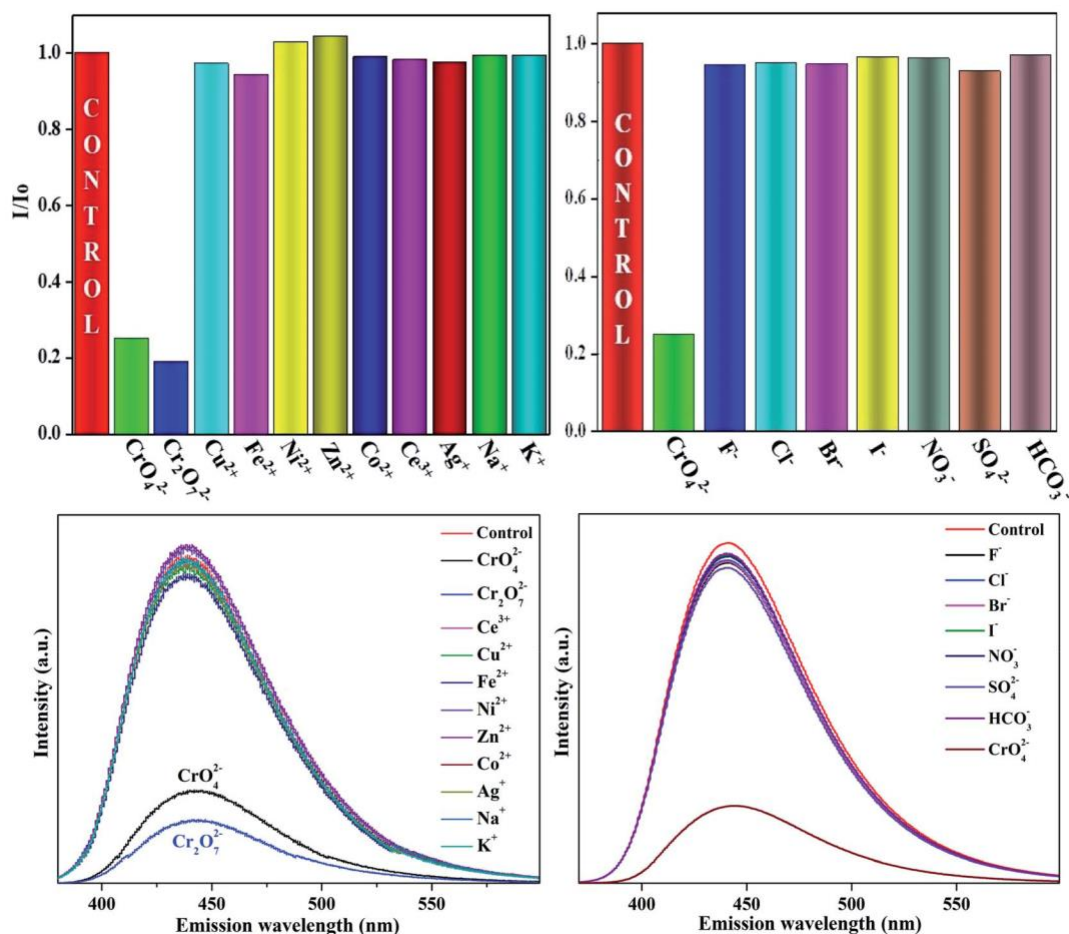

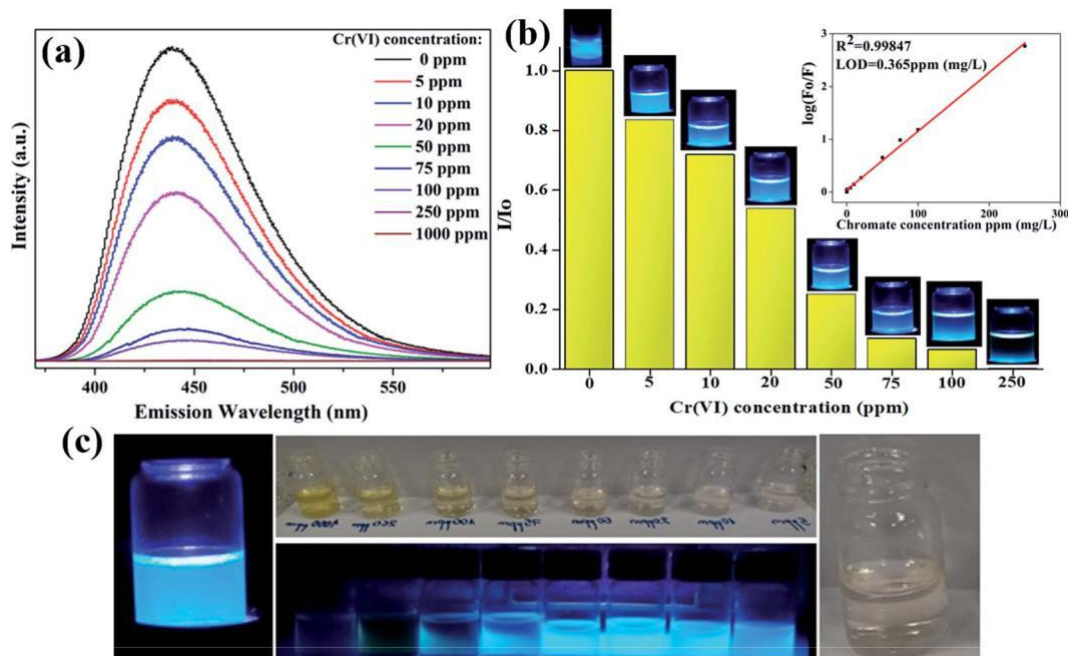Fig. 5 Selectivity of the N-doped CQDs based sensor over other ions and anions.

Fig. 6 Cr(VI) ions influence on PL spectrum of N-doped CQDs in (a and b) reflecting the intensity changes in ppm concentration range with (inset) showing Stem–Volmer plot, log(F_0/F) versus concentration and (c) photo of the effect of different Cr(VI) ions concentration on NCQDs emission under UV light.
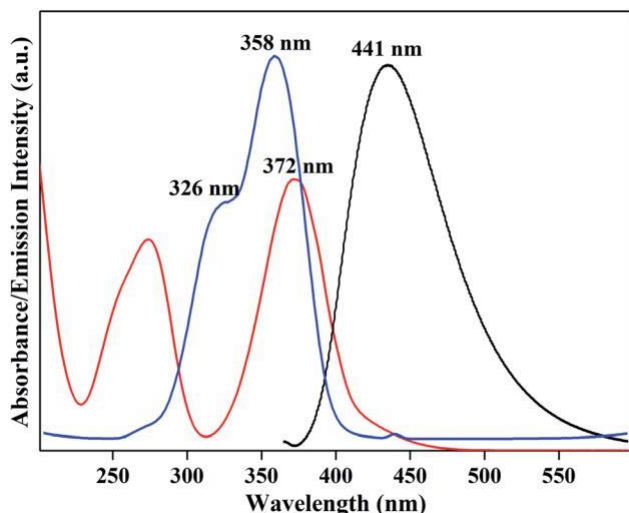

Fig. 7 The Inner Filter Effect of Chromate (CrO_4^2) representing the spectral overlap between the chromate normalised UV-Vis absorption band (red line), N-doped CQD's excitation spectrum (emission wavelength l_{em} ¼ 441 nm) (blue line), and the emission spectrum (excitation wavelength l_{ext} ¼ 360 nm) (black line).

UV-Vis spectra of the Cr(VI) and NCQDs mixture compared to Cr(VI) and NCQDs controls, suggests a mechanism other than that involving Cr(VI)-NCQD surface interactions. The selectivity of the CHFS-synthesised NCQD towards Cr(VI) can be attributed to the Inner Filter Effect (IFE). The IFE occurs where there exists a spectral overlap between the absorption bands of the chro-mate (CrO_4^2) and the excitation band and/or emission band of the NCQDs as shown in Fig. 7.

The excitation spectrum for the NCQDs has two overlapping bands at 326 nm and 358 nm with its emission band centred at 441 nm (excitation at 360 nm), whereas the chromate (CrO_4^2) has one of its absorption bands centred at 372 nm, with signi cant overlap of the maximum excitation band of the NCQDs. These factors generate an absorptive competition between anion units and NCQDs particles inside the solution, moreover, not only is the chromate effectively absorbing the radiation at 360 nm necessary for NCQDs to generate the transition to the excited state, but it can also absorb emitted light from the NCQDs, translating to a quenching of the NCQDs uorescence. The quenching mechanism, IFE, has been previ-ously reported as an effective on−off, rapid and enhanced sensitivity approach to chromium(VI) sensing.[33,46]

Conclusions

In conclusion, a continuous hydrothermal ow synthesis route was developed for the synthesis of carbon rich, nitrogen-doped carbon quantum dots starting from citric acid and ammonia as precursors. The photoluminescence studies for the NCQDs demonstrated excitation independent behaviour with the emission peak at 441 nm due to the diversity of functional groups surface coverage from N-doping of the CQDs. Further-more, we provide the proof of principle application that in aqueous solutions the materials display a high selectivity and sensitivity for Cr(VI), rendering our materials suitable for envi-ronmental applications. The materials may also be applied in a spectrum of applications including photovoltaics, bio-tagging, energy storage and beyond.

Conflicts of interest

The authors have no conﬂicts of interest to declare.

Acknowledgements

References

1 P. Zuo, X. Lu, Z. Sun, Y. Guo and H. He, Microchim. Acta, 2016, **183**, 519–542.

2 X. Luo, A. H. M. Al-Antaki, K. Vimalanathan, J. Moffatt, K. Zheng, Y. Zou, J. Zou, X. Duan, R. N. Lamb, S. Wang, Q. Li, W. Zhang and C. L. Raston, React. Chem. Eng., 2018, **3**, 164–170.

3 S. t. Yang, Li Cao, P. G. Luo, F. Lu, X. Wang, H. Wang, M. J. Meziani, Y. Liu, G. Qi and Y. Sun, J. Am. Chem. Soc., 2009, **131**, 11308–11309.

4 Z. Ma, H. Ming, H. Huang, Y. Liu and Z. Kang, New J. Chem., 2012, **36**, 861.

5 Q. Wang, X. Huang, Y. Long, X. Wang, H. Zhang, R. Zhu, L. Liang, P. Teng and H. Zheng, Carbon, 2013, **59**, 192–199.

6 H. Ding, F. Du, P. Liu, Z. Chen and J. Shen, ACS Appl. Mater. Interfaces, 2015, **7**, 6889–6897.

7 S. Qu, X. Wang, Q. Lu, X. Liu and L. Wang, Angew. Chem., Int. Ed., 2012, **51**, 12215–12218.

8 S. Zhu, Q. Meng, L. Wang, J. Zhang, Y. Song, H. Jin, K. Zhang, H. Sun, H. Wang and B. Yang, Angew. Chem., Int. Ed., 2013, **52**, 3953–3957.

9 K. Qu, J. Wang, J. Ren and X. Qu, Chem.–Eur. J., 2013, **19**, 7243–7249.

10 X. Guo, C.-F. Wang, Z.-Y. Yu, L. Chen and S. Chen, Chem. Commun., 2012, **48**, 2692.

11 H. Li, X. He, Z. Kang, H. Huang, Y. Liu, J. Liu, S. Lian, C. H. A. Tsang, X. Yang and S. T. Lee, Angew. Chem., Int. Ed., 2010, **49**, 4430–4434.

12 O. Mashtalir, M. R. Lukatskaya, M. Q. Zhao, M. W. Barsoum and Y. Gogotsi, Adv. Mater., 2015, **27**, 3501–3506.

13 J. Briscoe, A. Marinovic, M. Sevilla, S. Dunn and M. Titirici, Angew. Chem., Int. Ed., 2015, **54**, 4463–4468.

14 A. Marinovic, L. S. Kiat, S. Dunn, M. M. Titirici and J. Briscoe, ChemSusChem, 2017, **10**, 1004–1013.

15 S. Zhu, Y. Song, X. Zhao, J. Shao, J. Zhang and B. Yang, Nano Res., 2015, **8**, 355–381.

16 N. Papaioannou, A. Marinovic, N. Yoshizawa, A. E. Goode, M. Fay, A. Khlobystov, M. M. Titirici and A. Sapelkin, Sci. Rep., 2018, **8**, 6559.

17 F. Yuan, T. Yuan, L. Sui, Z. Wang, Z. Xi, Y. Li, X. Li, L. Fan, Z. Tan, A. Chen, M. Jin and S. Yang, Nat. Commun., 2018, **9**, 2249.

18 J. Zhang and S.-H. Yu, Mater. Today, 2016, **19**, 382–393.

19 R. Wang, K.-Q. Lu, Z.-R. Tang and Y.-J. Xu, J. Mater. Chem. A, 2017, **5**, 3717–3734.

20 F. Li, D. Yang and H. Xu, Chem.–Eur. J., 2019, **25**, 1165–1176.

21 J. A. Darr, J. Zhang, N. M. Makwana and X. Weng, Chem. Rev., 2017, **117**, 11125–11238.

22 C. J. Tighe, R. Q. Cabrera, R. I. Gruar and J. A. Darr, Ind. Eng. Chem. Res., 2013, **52**, 5522–5528.

23 J. A. Darr and M. Poliakoff, Chem. Rev., 1999, **99**, 495–542.

24 A. Cabanas, J. A. Darr, E. Lester and M. Poliakoff, J. Mater. Chem., 2001, **11**, 561–568.

25 V. Middelkoop, T. Slater, M. Florea, F. Neaţu, S. Danaci, V. Onyenkeadi, K. Boonen, B. Saha, I. A. Baragau and S. Kellici, J. Cleaner Prod., 2019, **214**, 606–614.

26 S. Kellici, J. Acord, A. Vaughn, N. P. Power, D. J. Morgan, T. Heil, S. P. Facq and G. I. Lampronti, ACS Appl. Mater. Interfaces, 2016, **8**, 19038–19046.

27 S. Kellici, J. Acord, K. E. Moore, N. P. Power, V. Middelkoop, D. J. Morgan, T. Heil, P. Coppo, I. A. Baragau and C. L. Raston, React. Chem. Eng., 2018, **3**, 949–958.

28 V. Middelkoop, C. J. Tighe, S. Kellici, R. I. Gruar, J. M. Perkins, S. D. M. Jacques, P. Barnes and J. A. Darr, J. Supercrit. Fluids, 2014, **87**, 118–128.

29 S. Kellici, J. Acord, N. P. Power, D. J. Morgan, P. Coppo, T. Heil and B. Saha, RSC Adv., 2017, **7**, 14716–14720.

30 J. B. M. Goodall, S. Kellici, D. Illsley, R. Lines, J. C. Knowles and J. a. Darr, RSC Adv., 2014, **4**, 31799–31809.

31 X. Gao, C. Du, Z. Zhuang and W. Chen, J. Mater. Chem. C, 2016, **4**, 6927–6945.

32 A. Iqbal, K. Iqbal, L. Xu, B. Li, D. Gong, X. Liu, Y. Guo, W. Liu, W. Qin and H. Guo, Sens. Actuators, B, 2018, **255**, 1130–1138.

33 M. Zheng, Z. Xie, D. Qu, D. Li, P. Du, X. Jing and Z. Sun, ACS Appl. Mater. Interfaces, 2013, **5**, 13242–13247.

34 Y. Dong, R. Wang, G. Li, C. Chen, Y. Chi and G. Chen, Anal. Chem., 2012, **84**, 6220–6224.

35 X. Wu, F. Tian, W. Wang, J. Chen, M. Wu and J. X. Zhao, J. Mater. Chem. C, 2013, **1**, 4676.

36 A. Zhitkovich, Chem. Res. Toxicol., 2011, **24**, 1617–1629.

37 M. Costa and C. B. Klein, Crit. Rev. Toxicol., 2006, **36**, 155–163.

38 C. Pellerin and S. M. Booker, Environ. Health Perspect., 2000, **108**, 402–407.

39 D. J. Paustenbach, B. L. Finley, F. S. Mowat and B. D. Kerger, J. Toxicol. Environ. Health, Part A, 2003, **66**, 1295–1339.

40 S. H. Jin, D. H. Kim, G. H. Jun, S. H. Hong and S. Jeon, ACS Nano, 2013, **7**, 1239–1245.

41 P. Lazar, R. Mach and M. Otyepka, J. Phys. Chem. C, 2019, **123**, 10695–10702.

42 M. Zhou, Z. Zhou, A. Gong, Y. Zhang and Q. Li, Talanta, 2015, **143**, 107–113.

43 C. Yang, S. Zhu, Z. Li, Z. Li, C. Chen, L. Sun, W. Tang, R. Liu, Y. Sun and M. Yu, Chem. Commun., 2016, **52**, 11912–11914.

44 Y. Dong, H. Pang, H. Bin Yang, C. Guo, J. Shao, Y. Chi, C. M. Li and T. Yu, Angew. Chem., Int. Ed., 2013, **52**, 7800–7804.

45 H. Ding, S. B. Yu, J. S. Wei and H. M. Xiong, ACS Nano, 2016, **10**, 484–491.

46 S. Huang, H. Qiu, F. Zhu, S. Lu and Q. Xiao, Microchim. Acta, 2015, **182**, 1723–1731.